Behavioral/Systems/Cognitive

$P2Y_1$ Receptor Modulation of the Pre-Bötzinger Complex Inspiratory Rhythm Generating Network *In Vitro*

Amanda R. Lorier,[1,2] Adrianne G. Huxtable,[1] Dean M. Robinson,[2] Janusz Lipski,[2] Gary D. Housley,[2] and Gregory D. Funk[1,2]

[1]Department of Physiology, Faculty of Medicine and Dentistry, University of Alberta, Edmonton, Alberta, Canada T6G 2H7, and [2]Department of Physiology, Faculty of Medicine and Health Sciences, University of Auckland, Auckland, Private Bag 92019, New Zealand

ATP is released during hypoxia from the ventrolateral medulla (VLM) and activates purinergic P2 receptors (P2Rs) at unknown loci to offset the secondary hypoxic depression of breathing. In this study, we used rhythmically active medullary slices from neonatal rat to map, in relation to anatomical and molecular markers of the pre-Bötzinger complex (preBötC) (a proposed site of rhythm generation), the effects of ATP on respiratory rhythm and identify the P2R subtypes responsible for these actions. Unilateral microinjections of ATP in a three-dimensional grid within the VLM revealed a "hotspot" where ATP (0.1 mM) evoked a rapid 2.2 ± 0.1-fold increase in inspiratory frequency followed by a brief reduction to 0.83 ± 0.02 of baseline. The hotspot was identified as the preBötC based on histology, overlap of injection sites with NK1R immunolabeling, and potentiation or inhibition of respiratory frequency by SP ([Sar^9-$Met(O_2)^{11}$]-substance P) or DAMGO ([D-Ala^2,*N*-$MePhe^4$,$Gly\text{-}ol^5$]-enkephalin), respectively. The relative potency of P2R agonists [2MeSADP (2-methylthioadenosine 5′-diphosphate) ≈ 2MeSATP (2-methylthioadenosine 5′-triphosphate) ≈ ATPγs (adenosine 5′-[γ-thio]triphosphate tetralithium salt) ≈ ATP ≫ UTP ≈ αβmeATP (α,β-methylene-adenosine 5′-triphosphate)] and attenuation of the ATP response by MRS2179 (2′-deoxy-N^6-methyladenosine-3′,5′-bisphosphate) ($P2Y_1$ antagonist) indicate that the excitation is mediated by $P2Y_1$Rs. The post-ATP inhibition, which was never observed in response to ATPγs, is dependent on ATP hydrolysis. These data establish in neonatal rats that respiratory rhythm generating networks in the preBötC are exquisitely sensitive to $P2Y_1$R activation, and suggest a role for $P2Y_1$Rs in respiratory motor control, particularly in the P2R excitation of rhythm that occurs during hypoxia.

Key words: **purine receptor; neonatal rat; ATP; adenosine; substance P; immunohistochemistry**

Introduction

ATP, best known as an energy substrate in virtually all cells, is also a neurotransmitter that activates ionotropic ($P2X_{1-7}$) and metabotropic ($P2Y_{1,2,4,6,11-14}$) purinergic receptors (P2Rs) (Illes and Alexandre Ribeiro, 2004). The widespread expression of P2Rs in the nervous system (Collo et al., 1996; Kanjhan et al., 1999; Norenberg and Illes, 2000; Yao et al., 2000) and extensive electrophysiological evidence (Norenberg and Illes, 2000; Hussl and Boehm, 2006; North and Verkhratsky, 2006) support diverse functions for P2R signaling. Recent discoveries have focused attention on the role of P2Rs in respiratory control. First, P2Rs are expressed in respiratory regions of the PNS and CNS, including the carotid body, petrosal ganglion (Prasad et al., 2001; Rong et al., 2003), brainstem respiratory nuclei (Kanjhan et al., 1999; Yao et al., 2000; Thomas et al., 2001), and respiratory motoneurons (Funk et al., 1997a; Kanjhan et al., 1999; Miles et al., 2002). Second, $P2X_2$Rs in the carotid body are necessary for the hypoxic ventilatory response (Rong et al., 2003). Most recently, biosensor data have revealed that ATP is released from discrete regions in the brainstem in response to hypercapnia or hypoxia and that the subsequent activation of P2Rs contributes to the associated respiratory responses (Gourine et al., 2005a,b).

The underlying mechanisms are not known, but distinct spatiotemporal patterns of ATP release in hypercapnia and hypoxia produce diverse actions. ATP release from the ventral medullary surface is common to hypoxia and hypercapnia, but ATP release from the ventral respiratory column (VRC) occurs in hypoxia only (Gourine et al., 2005a,b). In addition, ATP release in hypoxia is delayed relative to hypercapnia, occurring shortly after the initial increase in respiratory frequency when it attenuates the secondary hypoxic depression of ventilation (Gourine et al., 2005a). Based on the observations that the ATP component of the respiratory response to hypoxia is to increase frequency, and that ATP is released within the VRC only during hypoxia (Gourine et al., 2005a), we hypothesize that ATP acts directly in the VRC to stimulate frequency. Few data address this question. In the adult rat *in vivo*, ATP increases the discharge of brainstem respiratory neurons (Thomas and Spyer, 2000) but blocks phrenic nerve output causing apnea (Spyer and Thomas, 2000; Gourine et al., 2005b). In the neonatal rat *in vitro*, ATP increases respiratory frequency (Lorier et al., 2002, 2004). However, comparison is difficult because the site(s) of drug action were poorly defined,

Received June 21, 2006; revised Nov. 21, 2006; accepted Dec. 13, 2006.

This work was supported by the Alberta Heritage Foundation for Medical Research (AHFMR), Canadian Institute for Health Research, Canadian Foundation for Innovation, Alberta Science and Research Authority, Health Research Council of New Zealand (HRC), and Auckland Medical Research Foundation (AMRF). A.R.L. was supported by studentships from HRC and AMRF. G.D.F. is a Senior Scholar of the AHFMR. We thank Drs. Silvia Pagliardini and John Greer for their invaluable assistance with immunohistochemistry.

Correspondence should be addressed to Dr. Gregory D. Funk, 7-50 Medical Sciences Building, Department of Physiology, University of Alberta, Edmonton, Alberta, Canada T6G 2H7. E-mail: gf@ualberta.ca.

DOI:10.1523/JNEUROSCI.3948-06.2007

 0270-6474/07/270993-13$15.00/0

and the experimental conditions and models (adults *in vivo* vs neonates *in vitro*) differed.

The objectives of this study are to explore mechanisms by which ATP modulates respiratory rhythm. We will (1) map, in relation to anatomical and molecular markers of medullary respiratory nuclei, the effects of ATP on respiratory rhythm and identify the site where ATP maximally increases frequency (ATP "hotspot"); (2) test whether the ATP hotspot corresponds to the pre-Bötzinger complex (preBötC) (a proposed site of inspiratory rhythm generation); and (3) identify the P2R subtype(s) responsible for the ATP-mediated increase in respiratory frequency.

Materials and Methods

Rhythmically active medullary slice. Rhythmically active medullary slices ($n = 145$) were obtained from neonatal [postnatal day 0 (P0) to P4] Wistar rats as described previously (Smith et al., 1991; Funk et al., 1993, 1997b). Briefly, animals were anesthetized through inhalation of ether or isoflurane and decerebrated. The brainstem–spinal cord was then isolated in cold artificial CSF (aCSF) containing the following (in mM): 120 NaCl, 3 KCl, 1.0 $CaCl_2$, 2.0 $MgSO_4$, 26 $NaHCO_3$, 1.25 NaH_2PO_4, 20 D-glucose, equilibrated with 95% O_2/5% CO_2. The brainstem–spinal cord was pinned to a wax chuck, and serial 100–200 μm sections were cut in the rostral-to-caudal direction using a vibratome (Pelco-101; Ted Pella, Redding, CA; or VT1000S, Leica, Nussloch, Germany) and transilluminated to identify anatomical landmarks. A single 700 μm slice was cut after the cNA (compact division of nucleus ambiguus) was no longer evident and the rostral margin of the inferior olive first appeared in the thin sections. The 700 μm rhythmic slice extended from the rostral margin described above to the obex caudally and contained the preBötC, rVRG (rostral ventral respiratory group), most of the XII motor nuclei, and the rostral XII nerve rootlets. Slices were pinned with the rostral surface up on Sylgard resin in a recording chamber (volume, 5 or 10 ml) and perfused with aCSF that was recirculated at a flow rate of 15–20 ml/min. The concentration of K^+ in the aCSF ($[K^+]_e$) was raised from 3 to 9 mM at least 30 min before the start of data collection (Funk et al., 1993). Elevated $[K^+]_e$ is not a necessary condition for rhythm generation, despite a common misconception to the contrary. Medullary slices from neonatal Wistar rats that are 700 μm thick generate stable respiratory rhythm in 3 mM $[K^+]_e$ for 2 h on average, after which rhythm gradually slows over the next 2 h and then ceases (Ruangkittisakul et al., 2006). However, the majority of protocols in this study involved multiple interventions, and therefore required slices that produced stable inspiratory-related rhythm for extended periods (i.e., >5 h). Therefore, the $[K^+]_e$ was raised from 3 to 9 mM. It has been hypothesized that the rundown of rhythmic activity in medullary slices is attributable to the removal of tonic excitatory inputs or washout of an excitatory modulator that normally maintains the excitability of a critical population of neurons at a level necessary for long-term rhythm generation (Smith et al., 1991). Elevated $[K^+]_e$ is proposed to compensate for the loss of this excitatory/modulatory input (for additional discussions, see Funk et al., 1993; Ruangkittisakul et al., 2006).

All experiments and procedures were approved by the University of Auckland and/or University of Alberta Animal Ethics Committees and performed in accordance with their guidelines for the care, handling, and treatment of experimental animals.

Electrophysiological recordings. Inspiratory activity was recorded, using glass suction electrodes (A-M Systems, Carlsborg, WA), from cut ends of XII (hypoglossal) nerve rootlets and directly from the ventrolateral surface of the slice. Surface field potentials were recorded using a four-axis manual manipulator to place a suction electrode (120 μm inside diameter) on the surface of the slice over the approximate region of the ventral respiratory cell column (Telgkamp and Ramirez, 1999). The pipette was systematically moved in steps corresponding to one-half of the pipette diameter until the most robust signal was detected. Signals were amplified, bandpass filtered (100 Hz to 5 kHz), full-wave rectified, integrated using a leaky integrator ($\tau = 25$ or 50 ms), and displayed using Axoscope 9.0 (Molecular Devices, Union City, CA). Data were recorded on videotape via pulse code modulation (Vetter model 402 or 3000A; A. H. Vetter, Rebersburg, PA) or saved to computer using a Digidata 1322 A/D board and AxoScope software (Molecular Devices) for off-line analysis. All recordings were conducted at room temperature (22–24°C).

Drugs and their application. Stock solutions of drugs were made in standard aCSF and frozen in aliquots unless otherwise stated. The final concentration of K^+ in the drug solutions was matched to that of the aCSF.

The following drugs were used: adenosine 5′-triphosphate disodium salt (ATP) (P2R agonist; 0.01–10 mM; made fresh on the day of experiment); adenosine 5′-[γ-thio]triphosphate tetralithium salt (ATPγs) (nonhydrolyzable ATP analog and P2R agonist; 0.1 mM); α,β-methylene-adenosine-5′-triphosphate ($\alpha\beta$meATP) ($P2X_{1,3}R$ agonist; 0.1 mM); 2-methylthioadenosine 5′-triphosphate (2MeSATP) ($P2X_{2,4,5}$ and $P2Y_1R$ agonist; 0.1 mM); 2-methylthioadenosine 5′-diphosphate (2MeSADP) ($P2Y_1R$ agonist; 0.1 mM); pyridoxal-phosphate-6-azophenyl-2′,4′-disulfonic acid 4-sodium (PPADS) (10–500 μM); $CuCl_2$ (10–50 μM; Fisher Scientific, Houston, TX); suramin (10–50 μM); uridine 5′-triphosphate trisodium salt (UTP) (P2YR agonist; 0.1 mM) (all from Sigma, St. Louis, MO); [Sar^9-Met(O_2)^{11}]-substance P (SP) (NK1R agonist; 1 μM); DAMGO (μ-opioid receptor agonist; 50 μM); 2′-deoxy-N^6-methyladenosine-3′,5′-bisphosphate (MRS2179) ($P2Y_1R$ antagonist; 50–100 μM); 2′,3′-*O*-(2,4,6-trinitrophenyl)-ATP (TNP-ATP) ($P2X_{1,3}R$ antagonist; 10 nM to 10 μM) (all from Tocris, Ellsville, MO).

Drugs were either bath-applied or microinjected via triple-barreled pipettes (5–6 μm per barrel outer diameter pulled from borosilicate glass capillaries) (World Precision Instruments, Sarasota, FL). Care was taken to ensure that pipette tip diameter fell within this range, because examination of Lucifer yellow-filled triple-barreled pipettes under a fluorescent microscope (40× objective) revealed that pipettes of this range did not leak, but they did leak if tip diameter exceeded 6.5 μm. Avoiding leakage was essential because of the potential for agonist evoked P2R desensitization or internalization, and observations in preliminary experiments with larger pipettes showed that ATP responses were either absent or not repeatable. As an additional step to minimize the confounding influence of drug leakage, the pipette was removed from the injection site to the solution above the slice in the time between consecutive injections. Drug microinjections (~10 psi) were controlled via a programmable stimulator (Master-8; AMPI Instruments, Jerusalem, Israel) linked to a solenoid. Consecutive agonist applications were separated by an interval of at least 15 min. We did not systematically assess whether this was the minimum time interval required for consistent responses, but it was sufficient for reproducible responses.

The concentration of agonists used to evoke responses was higher than that used in expression systems or on isolated cells. This is consistent with the majority of the literature indicating that the concentration of P2R agonists required to evoke P2R currents in neurons in slices is much higher than required in dissociated cells or expression systems (North, 2002). This is likely attributable to reduced penetration of agonist through the tissue, degradation of ATP in slices by ectonucleotidases, or receptor desensitization/internalization in response to ATP released during the preparation of the brain slice (North, 2002). An additional factor is that when drugs are microinjected locally from a drug pipette, the concentration of drug decreases exponentially with distance from the pipette tip (Nicholson, 1985). Previous work using *in vitro* preparations similar to those used here, indicates that to produce similar effects, the concentration of drug in the pipette must be ~10-fold higher than the concentration in the bath (Liu et al., 1990). Therefore, drug concentrations used in our experiments should not be directly compared with studies in which the same agents are bath-applied to isolated cells.

ATP microinjection mapping studies. Preliminary experiments mapping the effects on rhythm of microinjecting ATP into the ventrolateral medulla (VLM) suggested that the potentiation of frequency by ATP occurs within a limited region of the medullary slice in the vicinity of the ventral medullary respiratory group. Subsequent experiments were therefore performed in reference to a suction electrode placed on the rostral surface of the slice over the preBötC region where a large amplitude rhythmic inspiratory-related field potential was recorded.

Mapping studies were performed using 10 s applications of 0.1 mM ATP. ATP responses were first mapped along the mediolateral (x) axis

starting at the level on the dorsoventral (*y*) axis of the surface suction electrode. The pipette tip was ~150 μm below the slice surface (depth corresponds to the *z*-axis). ATP was injected, and the response was recorded. The pipette was then moved in steps of 75 or 150 μm along the *x*-axis. Microinjections were repeated at 15 min intervals until the most potent frequency response was evoked. The pipette was then returned to the site of maximum ATP sensitivity (on the *x*-axis), and the procedure was repeated (at 75 μm intervals) along the dorsoventral (*y*) axis. Physical interference between the surface extracellular electrode and the injection pipette prevented microinjections >150 μm lateral to the hotspot. Once the ATP hotspot was identified along *x*- and *y*-axes, ATP was injected at two different depths along the rostrocaudal (*z*) axis. Note that spatial resolution in the *z*-axis with this procedure was limited compared with *x*- and *y*-axes because of the potential for the injected drug to move up the electrode track (i.e., the deeper drug injections may affect more tissue). Therefore, to further assess whether the sensitivity of respiratory networks to ATP varies along the rostrocaudal axis, an additional series of experiments was conducted in which the ATP hotspot was first mapped with the rostral surface of the slice mounted upward. The slice was then flipped over, the respiratory cell column was located on the caudal surface using a suction electrode, and the ATP hotspot was mapped along *x*- and *y*-axes as described above, with drug pipette tip ~150 μm below the slice surface (i.e., ~ 400 μm caudal to the rostral map).

Histology. Iontophoretic application (−10 mA; 3 s on/3 s off for a total of 15 min) of pontamine sky blue (2%; dissolved in sodium acetate; Sigma) was used in the mapping experiments to label the site at which ATP produced the largest increase in frequency. While pontamine sky blue was contained in a separate microelectrode than that used to microinject drugs, placement of the dye pipette in the same site as the drug pipette was accomplished using micrometers on each of the four manipulator axes. After iontophoresis, the slice was fixed in 4% formaldehyde/phosphate buffer (PB) overnight and cryoprotected in 30% sucrose. These 700 μm rhythmic slices were then sectioned at 50 μm on a cryostat. Sections were mounted onto slides, air dried, stained with cresyl violet, dehydrated, and coverslipped with Permount (Biomeda, Foster City, CA). Remaining sections were placed in 48-well plates for immunohistochemical analysis.

Although inclusion of dye with the injected drug can be used to estimate the degree of drug diffusion and the region of tissue affected, this was not done for two reasons. First, marker dyes often do not have the same diffusion coefficient as the agonist. Second, and most importantly, extracellular ATP is rapidly hydrolyzed by ectonucleotidases, which means that measuring the distance over which a marker dye diffuses is likely to overestimate, perhaps dramatically, the area actually affected by ATP. Some insight into the degree of diffusion, however, can be obtained from the mapping studies that defined how the effects of ATP on rhythm changed as a function of distance from the hotspot.

Immunohistochemistry. The pattern of NK1R expression in relation to the pontamine sky blue-labeled injection site was assessed via immunohistochemistry. Free-floating, 50 μm sections were washed in PBS for 30 min, incubated in 1% H_2O_2 for 30 min, washed in PBS (three times, 15 min each time), blocked with 2% bovine serum albumin (BSA) (Sigma) and 1% Triton X-100 (in PBS, used to permeabilize membranes) for 2 h, and then incubated overnight at room temperature in rabbit anti-NK1R antibody (1:1000; Advanced Targeting Systems, San Diego, CA). Sections were then rinsed in PBS (three times, 45 min each time), incubated in biotinylated donkey anti-rabbit antibody (1:1000) and 1% BSA for 2 h, washed in PBS (three times, 30 min each time), incubated in ABC Elite reagent (Vector Laboratories, Burlingame, CA) for 1.5 h, washed twice in PBS (15 min each) and once in Tris-HCl (15 min), and reacted with a solution containing 0.3 mg/ml DAB and 1% H_2O_2/Tris-HCl. After a final wash in PBS, sections were mounted on slides and coverslipped with Permount (Biomeda).

To examine $P2X_2$ and $P2Y_1$ receptor expression in relation to NK1 receptor expression in the neonatal rat preBötC, animals (P0–P3) were anesthetized deeply with isoflurane and perfused transcardially with 4% paraformaldehyde in 0.1 M PB. Brainstems were removed, postfixed overnight in 4% paraformaldehyde, and sliced into 50 μm sections on a Leica VT 1000S vibratome. Sections were stored in 0.01% sodium azide in PB until processed for immunohistochemisty.

Immunohistochemistry for the $P2X_2$ ($n = 4$) and $P2Y_1$ receptors ($n = 4$) was performed using the PerkinElmer (Boston, MA) Renaissance TSA Fluorescence Systems Tyramide Signal Amplification Protocol (NEL701A). Virtually identical procedures were used to examine immunolabeling for both receptors in relation to NK1 receptor expression in the preBötC of neonatal rats. The main exception was that for $P2X_2$ labeling, the rabbit anti-$P2X_2$R antibody was the first primary antibody, whereas for $P2Y_1$ labeling, the rabbit anti-NK1R antibody was used first. In brief, all sections were initially washed three times with 0.1 M PBS. Endogenous peroxidase activity was quenched by 20 min incubation with 1% H_2O_2. After PBS washes, sections were placed in 0.3% Triton X-100 in TNB (0.1 M Tris-HCl, pH 7.5, 0.15 M NaCl, 0.5% blocking reagent, supplied in kit) buffer for 1 h to decrease nonspecific staining and increase antibody penetration. Sections were then incubated in the first primary antibody (either rabbit anti-$P2X_2$R; 1:3000; Alomone, Jerusalem, Israel; or rabbit anti-NK1R antibody; 1:30,000; Advanced Targeting Systems) and 0.3% Triton-X100 in TNB buffer overnight. After this first primary antibody incubation, sections were washed in TNT (0.1 M Tris-HCl, pH 7.5, 0.15 M NaCl, 0.05% Tween 20) buffer and incubated with biotin-SP-conjugated AffiniPure donkey anti-rabbit IgG (H+L) (1:200; Jackson ImmunoResearch Laboratories, West Grove, PA) in TNB buffer for 2 h. After washes in TNT buffer, sections were incubated with streptavidin-HRP (1:150) for 1 h, washed in TNT buffer, incubated for 10 min in Fluorescein Tyramide Reagent (1:75) Amplification Diluent, and washed again in TNT buffer. In preparation for the application of the second primary antibody, sections were again blocked in TNB buffer. Sections were then incubated overnight in the second primary antibody (either rabbit anti-NK1R antibody; 1:1000; Advanced Targeting Systems; or rabbit anti-$P2Y_1$R antibody; 1:100; Alomone), washed in TNT buffer, incubated for 2 h with Cy3-conjugated AffiniPure donkey anti-rabbit IgG (H+L) (1:200; Jackson ImmunoResearch Laboratories), washed again in TNT buffer and PBS, and then mounted on slides and coverslipped with Calbiochem (La Jolla, CA) Fluorsave Reagent.

Immunofluorescence images (1024 × 1024 pixels) were acquired with a Zeiss (Oberkochen, Germany) LSM 510 confocal laser-scanning system using an Axiovert 100M microscope and the following objectives: Fluar 10× [numerical aperture (NA), 0.5], Fluar 20× (NA, 0.75), or Plan-Neofluar 40× (NA, 1.3). Images were exported to Adobe Photoshop, version 7.0, and adjusted for contrast and brightness.

Data analysis. The effects of a drug on frequency of integrated inspiratory bursts recorded via suction electrodes from XII nerve roots and the preBötC were assessed off-line using custom-written LabVIEW acquisition and analysis protocols (Funk et al., 1997a; Miles et al., 2002) or pClamp 9.0 (Clampfit) and Microsoft Excel software. Values of frequency and amplitude during the drug were compared with the average value during the 90 s control period that immediately preceded drug application. The maximum effect of a drug on frequency was determined as the maximum (or minimum) value measured in the moving average of inspiratory frequency (calculation based on the average of four consecutive events) during the first minute after injection. The time course of the response was obtained by averaging data points in 30 s bins for the 1 min period immediately before drug application, in 10 s bins for the first 30 s after the onset of drug application, and in 30 s bins for the remainder of the time.

Parameters are reported in absolute terms, or relative to control (predrug or prestimulus) levels, as mean ± SE. All statistical analyses were performed on raw data. Differences between means were identified using the Student's *t* test when only two groups were compared. When more than two groups were compared, ANOVA with Bonferroni's or Dunnett's multiple comparison tests was used (GraphPad Prism 4.0). Values of $p < 0.05$ were assumed significant.

Results

P2R activation in discrete regions of the ventral medulla increases inspiratory frequency

Mapping studies identified a circumscribed region within the VLM where microinjection of ATP evoked a significantly greater

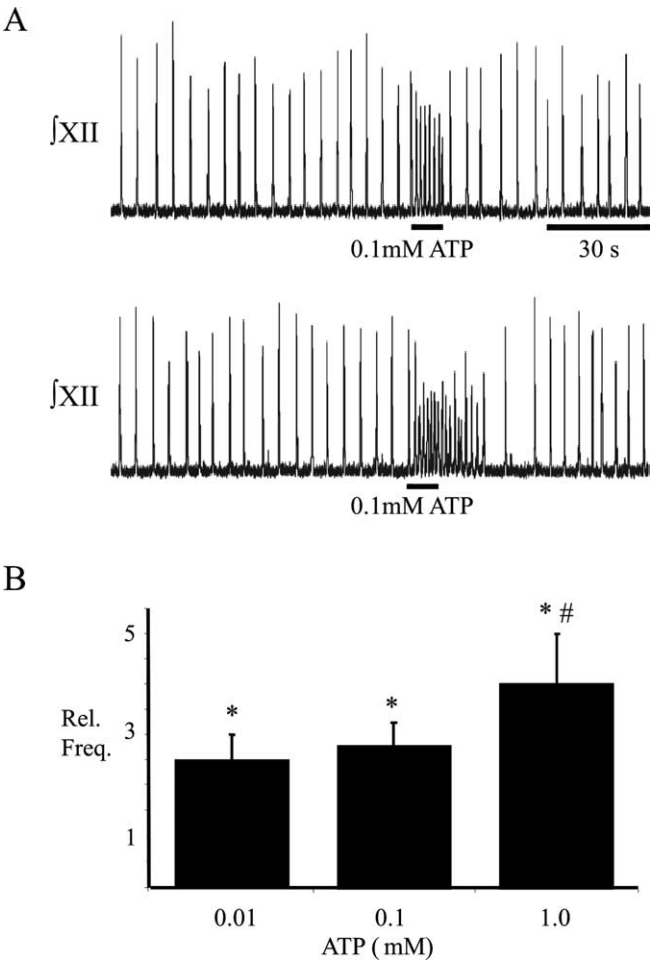

Figure 1. Potentiation of frequency by ATP is dose dependent. ***A***, ∫XII nerve recordings from a medullary slice preparation illustrating the response to local application of 0.01 and 0.1 mM ATP to site of maximum ATP sensitivity in the VLM. ***B***, Group data showing the dose-dependent effects of ATP (0.01, 0.1, and 1 mM; $n = 5$, 6, and 4, respectively) on frequency. Rel. Freq., Relative frequency. *Significantly different from control; #significantly different from 0.01 mM ATP response. Error bars indicate SEM.

increase in frequency compared with surrounding areas. As shown for an individual slice and population data, responses evoked by ATP in this hotspot were dose dependent. ATP increased frequency significantly by 2.44 ± 0.54-, 2.73 ± 0.50-, and 3.95 ± 1.04-fold with 0.01 mM ($n = 5$), 0.1 mM ($n = 6$), and 1 mM ATP ($n = 4$), respectively (Fig. 1). Responses evoked by ATP (10 s; 0.1 mM) in this hotspot were also remarkably consistent in magnitude and time course, whether applied repeatedly in a single preparation or compared between preparations. The response peaked 4.9 ± 0.4 s after the onset of ATP microinjection at frequencies (35.2 ± 2 cycles/min) that were 2.16 ± 0.13-fold greater than control (13.2 ± 1 cycles/min; $n = 18$). Frequency remained significantly elevated at 20 s after the onset of drug microinjection (Fig. 2*C*) (see also Figs. 5*C*, 10*B*, 11*C*). It then declined briefly (for one or two cycles) in ~75% preparations and reached a nadir 30–40 s after drug onset before returning to control levels. Examples of this post-ATP inhibition for individual slice preparations are shown in Figure 1*A* (as well as in Figs. 2*A*, 3*A*, 5*A*, 7*A*, 11). Data from a small subset of these experiments ($n = 18$, 4 of which did not show a post-ATP inhibition) revealed a small but significant post-ATP decrease in frequency that averaged 0.83 ± 0.02 of control ($n = 18$).

The ATP-mediated increase in frequency decreased dramatically when microinjection sites were moved away from the hotspot (Fig. 2*A*,*B*). When microinjected 150 and 300 μm medial to the hotspot, responses decreased to 0.49 ± 0.06 and 0.17 ± 0.04, respectively, of the maximum response evoked at the hotspot (Fig. 2*B*). Similarly, responses to applications 150 μm lateral to the hotspot were 0.52 ± 0.07 of maximum (Fig. 2*B*). In the dorsoventral axis, responses decreased to 0.51 ± 0.07 and 0.38 ± 0.08 of maximum when the injections were made 75 and 150 μm ventral to the hotspot and to 0.62 ± 0.09 and 0.20 ± 0.06 of maximum when injections were 75 or 150 μm dorsal to the hotspot (Fig. 2*B*).

Response kinetics was also much slower when ATP was microinjected away from the hotspot. When microinjected 150 μm from the hotspot along either the mediolateral (*x*)- or dorsoventral (*y*)-axes, the time to peak was increased significantly to 10.2 ± 1.4 and 8.6 ± 1.3 s, respectively (Fig. 2*C*).

The hotspot identified in this first experimental series was localized only in two dimensions (i.e., in *x*–*y* plane at a single rostrocaudal level). The hotspot corresponded closely to the region from which the strongest respiratory field potential could be recorded. Thus, to test whether the high sensitivity of this region 150 μm below the rostral surface was specific to that locus or a general response associated with activation of P2Rs in the ventral respiratory group, ATP was injected at two different points on the rostrocaudal (*z*) axis, 75 and 150 μm below the rostral surface. Frequency increased 2.00 ± 0.2-fold ($n = 4$) (data not shown) when ATP was injected 150 μm below the surface. This response was significantly greater than at the more rostral injection site (~75 μm below the rostral surface) where frequency increased 1.49 ± 0.07-fold.

It remained possible, however, that the greater response evoked at 150 μm simply reflected the activation of a greater volume of neural tissue because of the retrograde movement of drug up the 150 vs 75 μm electrode tract. To address this possibility, the ATP-sensitive site was mapped at a depth of 150 μm from one surface of the slice, the slice was flipped over and the other surface mapped. The hotspot on both surfaces mapped consistently to the region in the *x*–*y* plane that gave the largest inspiratory field potential. However, the increase in frequency evoked by ATP at the caudal site, which was ~400 μm caudal to the rostral site, was significantly less (2.1 ± 0.2-fold; $n = 7$) than obtained at the rostral site (2.8 ± 0.1-fold) (data not shown). This result was the same regardless of which surface was mapped first.

Because elevations in $[K^+]_e$ from 3 to 9 mM affect ion gradients, activity of ion pumps, reversal potential for K^+ currents, and therefore the actions of some neuromodulators, an additional series of experiments was performed to test whether the potentiation of frequency by ATP is dependent on elevated $[K^+]_e$. The ATP-evoked frequency response of slices bathed in 3 and 9 mM $[K^+]_e$ were compared. Medullary slices produced robust inspiratory-related rhythm at a frequency of 5.16 ± 0.4 cycles/min at 3 mM $[K^+]_e$ that increased to 9.09 ± 0.9 cycles/min in 9 mM $[K^+]_e$ ($n = 5$) (Fig. 3*A*). We used 0.05 mM ATP to ensure that the effect of ATP in 9 mM $[K^+]_e$ was not saturating. The relative effects on frequency of microinjecting ATP (0.05 mM) into the hotspot were similar in 3 and 9 mM $[K^+]_e$, increasing 2.79 ± 0.41- and 2.56 ± 0.33-fold, respectively (Fig. 3*B*).

ATP-induced increase in inspiratory frequency is mediated in the preBötC

Having mapped the ATP hotspot, we next used anatomical, molecular, and functional criteria that define the preBötC to test the

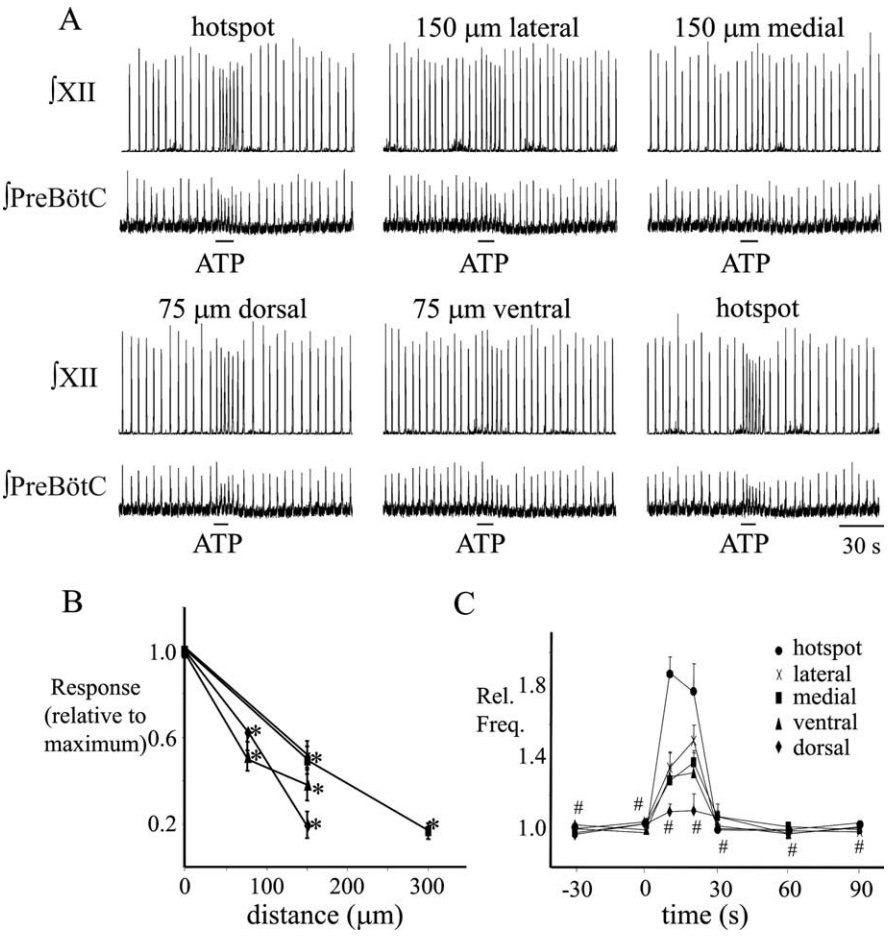

Figure 2. ATP potentiation of frequency is spatially restricted. ***A***, Integrated XII nerve (∫XII) and surface preBötC field potential (∫preBötC) recordings from a medullary slice preparation illustrating the effects on inspiratory-related output of locally applying 0.1 mM ATP at the site of maximum sensitivity in the VLM (the hotspot) and at sites of varying distances from the hotspot. ***B***, Group data illustrating the ATP responses, relative to the maximum response at the hotspot, evoked along different axes (indicated by different symbols) at various distances from hotspot. ***C***, The time course of the response to ATP application at the hotspot and at sites 150 μm distant in the lateral, medial, dorsal, or ventral directions. *Significantly different from maximum response; #not significantly different from control. Error bars indicate SEM.

hypothesis that the hotspot corresponds to the preBötC. For anatomical and molecular verification, mapping studies were concluded by marking the ATP hotspot via iontophoresis of pontamine sky blue ($n = 10$). This tissue was processed to establish the relationship between the hotspot and cytoarchitectural landmarks using cresyl violet and NK1R immunolabeling. A representative cresyl violet-labeled section and dye spot is shown in Figure 4, *A* and *B*. In the *x* and *y* plane of the slice, dye spots were mapped in relation to the semicompact nucleus ambiguus (scNA), the ventral and lateral surfaces of the section and midline (Fig. 4*C*). Dye spots clustered in a region ~200 μm ventral to the scNA, and ~700 μm lateral to the midline. In the rostocaudal (*z*) axis, dye spots were mapped according to the distance from the caudal margin of the VII nucleus, and the structure of the inferior olive (IO) complex. In this axis, dye spots clustered in a region that was between 400 and 500 μm caudal to the caudal margin of the facial nucleus, at the level where the dorsal (IOD) and principal nuclei of the IO (IOPr) fuse to form one continuous structure with three loops, and the ventral portion of the medial nucleus of inferior olive (IOM) is apparent.

To further assess whether the ATP hotspot corresponded to the preBötC, the spatial relationship between the pontamine sky blue dye spot and NK1R immunoreactivity (IR) was examined. Although NK1R-IR is not unique to the preBötC, it is noticeably more intense in the preBötC than in the adjacent reticular formation and is an established molecular marker of the preBötC (Gray et al., 1999; Guyenet and Wang, 2001; Wang et al., 2001). The most intense labeling was detected in the midline (Fig. 4*D*), consistent with previous observations that immature glial cells in the medullary midline express high levels of NK1-IR (Horie et al., 2000). Moderate NK1R-IR was also detected in the VLM in the region of the semicompact division of nucleus ambiguus (scNA) and regions ventral to the scNA that overlapped with pontamine sky blue injection sites (Fig. 4*D*). This was most obvious in higher magnification images of the ventrolateral region of the slice ipsilateral (Fig. 4*E*) and contralateral to the injection site (Fig. 4*F*). Note that the dense labeling typical of motoneurons of the compact NA (Pagliardini et al., 2003) was not apparent.

The hypothesis that the ATP hotspot corresponds to the preBötC was then tested functionally knowing that activation of NK1R or μ-opioid receptors in the preBötC increases or decreases burst frequency, respectively (Johnson et al., 1996; Gray et al., 1999). Using triple-barreled drug pipettes, the ATP hotspot was mapped as before. The NK1R agonist SP and the μ-opioid receptor agonist DAMGO were then locally injected into the ATP hotspot (Fig. 5*A*) ($n = 6$) at 15 min intervals. In this series, ATP (0.1 mM; 10 s) produced a rapid-onset, short-duration, 2.2 ± 0.14-fold increase in burst frequency that lasted for ~20 s. SP produced a rapid-onset, 2.3 ± 0.18-fold increase in frequency that peaked ~20 s after onset of SP application and lasted >30 s. DAMGO caused a dramatic reduction in frequency that reached a nadir at 0.37 ± 0.08 of control ~30 s after drug onset (Fig. 5*B*,*C*). This inhibitory action often took >7 min to washout.

Receptor subtypes responsible for the ATP-induced increase of inspiratory frequency

Based on immunohistochemical and electrophysiological evidence from the adult rat (Kanjhan et al., 1999; Yao et al., 2000; Thomas et al., 2001; Gourine et al., 2003) and the hypothesized importance of pH-sensitive, $P2X_2R$-mediated currents in central chemosensitivity (Thomas et al., 1999; Spyer and Thomas, 2000), we focused initially on the role of P2XRs, especially $P2X_2Rs$, in the ATP-mediated frequency response. Consistent with data from the adult rat (Kanjhan et al., 1999; Yao et al., 2000; Thomas et al., 2001; Gourine et al., 2003), immunolabeling for the $P2X_2R$ subunit was apparent in regions of the VLM (Fig. 6) that were, based on local anatomical landmarks and the presence of NK1R immunolabeling, consistent with the preBötC. High magnification revealed preBötC neurons that were im-

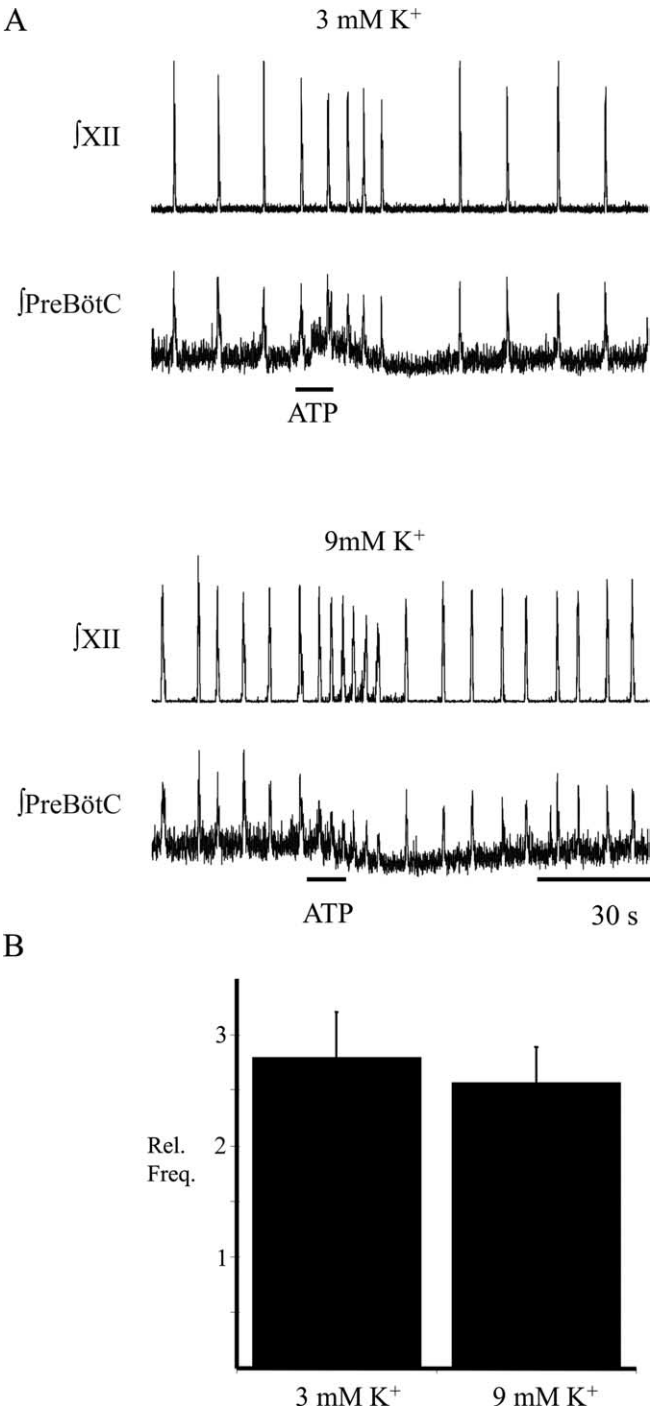

Figure 3. ATP-mediated potentiation of frequency is not affected by $[K^+]_e$. ***A***, ∫XII nerve and ∫preBötC recordings illustrating the effect of locally applying 0.05 mM ATP to the preBötC in 3 and then 9 mM $[K^+]_e$. Group data ($n = 5$) are shown in ***B***. Rel. Freq., Relative frequency. Error bars indicate SEM.

munofluorescent for $P2X_2$ (Fig. 6*D*), NK1 (Fig. 6*C*), or both $P2X_2$ and NK1Rs (Fig. 6*B*).

Based on the fact that only $P2X_2$ subunit-containing P2XRs are potentiated by acidic shifts in pH (King et al., 1997), we tested the involvement of $P2X_2$Rs in the ATP-evoked frequency increase by comparing ATP-evoked f responses at different levels of aCSF pH. In the first series, aCSF pH was changed from 7.56 ± 0.06 to 7.25 ± 0.01 by increasing the amount of CO_2 in the gas bubbling the aCSF. The effects of 0.1 mM ATP on frequency, however, were similar in 5% (2.68 ± 0.24-fold increase) and 10% CO_2 (2.30 ± 0.40-fold increase; $n = 3$) (data not shown). In the second series, the concentration of ATP was halved to 0.05 mM to address the possibility that the lack of a pH effect reflected that the response to 0.1 mM ATP was already maximal at 5% CO_2. The effects of ATP on frequency at 5% (2.07 ± 0.003) and 10% CO_2 (2.45 ± 0.23; $n = 3$) (data not shown) were still similar.

Finally, to address the possibility that the pH change had not been sufficient to potentiate $P2X_2$R-mediated responses, we compared the frequency response to ATP (0.1 mM, $n = 5$; 0.05 mM, $n = 6$; 0.01 mM, $n = 4$) over a greater pH range by reducing the concentration of $NaHCO_3$ in the aCSF bubbled with 10% CO_2 from 26 to 20 mM (low HCO_3^-). This produced a pH of 7.45 ± 0.01 in 5% CO_2 and 7.04 ± 0.02 in 10% CO_2/low HCO_3^-. However, the frequency response at each concentration remained insensitive to pH (Fig. 7) (i.e., frequency responses were insensitive to pH over a tenfold range in ATP concentration).

P2R subtype was also explored by microinjecting from triple-barreled pipettes a variety of P2R agonists into the preBötC, as identified via the ATP mapping protocol. In this series of experiments, application of ATP (0.1 mM; 10 s) into the preBötC increased inspiratory frequency 2.53 ± 0.35-fold (Fig. 8*A*) ($n = 9$). The P2R agonist 2MeSATP (0.1 mM), which has potency at $P2X_1$, $P2X_2$, $P2X_3$, $P2X_5$, $P2X_{2/3}$, and $P2X_{1/5}$ receptors (Norenberg and Illes, 2000; North and Surprenant, 2000), as well as $P2Y_1$, $P2Y_2$, $P2Y_6$, $P2Y_{11}$, $P2Y_{12}$, and $P2Y_{13}$ receptors (von Kugelgen and Wetter, 2000; von Kugelgen, 2005) produced an increase in frequency (2.96 ± 0.39-fold) similar to that of ATP (Fig. 8*A*) ($n = 4$). The $P2X_1$ and $P2X_3$ selective agonist $\alpha\beta$meATP (0.1 mM) (Norenberg and Illes, 2000) caused only a minor, but significant 1.2 ± 0.04-fold increase in frequency that reflected a remarkably consistent response between preparations (Fig. 8*A*) ($n = 5$). UTP, an agonist at $P2X_3$Rs and all P2YRs except $P2Y_1$ (von Kugelgen and Wetter, 2000), produced a minor, but significant, 1.55 ± 0.1-fold increase in frequency (Fig. 8*B*) when injected at sites where microinjection of ATP or SP potentiated respiratory frequency more than twofold (Fig. 8*B*) ($n = 6$). ATPγs, a hydrolysis-resistant agonist at $P2X_{1-6}$, $P2X_{2/3}$, $P2X_{1/5}$, $P2Y_1$, $P2Y_2$, $P2Y_4$, $P2Y_6$, and $P2Y_{11}$ receptors (Lambrecht, 2000), produced a 3.10 ± 0.3-fold increase in frequency in a series in which ATP caused a 3.30 ± 0.3-fold increase (Fig. 11) ($n = 7$). The general P2R antagonists, suramin and PPADS, did not significantly affect the ATP-mediated potentiation of inspiratory frequency. Suramin antagonizes $P2X_1$, $P2X_2$, $P2X_3$, $P2X_5$, $P2X_{2/3}$, $P2X_{1/5}$, $P2Y_{11}$, and $P2Y_{13}$ most potently but also $P2Y_1$ receptors at higher concentrations (Norenberg and Illes, 2000; von Kugelgen and Wetter, 2000). Given these broad actions, it was surprising that suramin did not reduce the ATP-evoked increase of inspiratory frequency (Fig. 8*C*) ($n = 4$). PPADS is generally more potent than suramin at P2XRs, antagonizing $P2X_1$, $P2X_2$, $P2X_3$, $P2X_5$, $P2X_{2/3}$, $P2X_{1/5}$, and also $P2Y_1$ receptors at higher concentrations (Norenberg and Illes, 2000; von Kugelgen and Wetter, 2000). Despite this, bath application of PPADS (50 μM) did not inhibit the ATP response. Frequency increased 2.24 ± 0.23 and 2.4 ± 0.11 (Fig. 8*D*) ($n = 5$) in control and in PPADS, respectively. Only when the concentration of PPADS was increased to 500 μM did its local pre-microinjection into the preBötC (2 min) partially block the ATP response from a 2.56 ± 0.2-fold increase in control to 1.79 ± 0.3 in PPADS (Fig. 8*E*) ($n = 5$). This could reflect antagonism of glutamate receptors, which can occur at such high concentrations of PPADS. However, the PPADS-mediated reduction in ATP sensitivity is more consistent with an inhibition of P2Rs, because the baseline frequency, which is dependent on glutamatergic

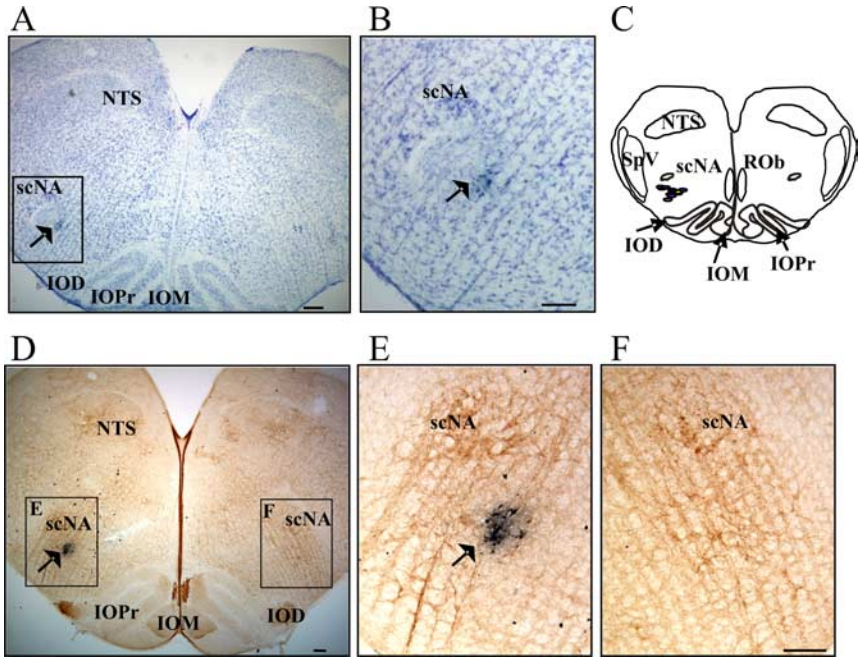

Figure 4. Anatomical identification of the ATP hotspot. ***A***, Photomicrograph of a cresyl violet-stained, transverse medullary section (50 μm) showing the location of pontamine sky blue-labeled (arrow) hotspot. ***B***, Higher magnification image of the boxed region in ***A***. ***C***, Schematic diagram of a transverse medullary section onto which the pontamine sky blue dye spots (ATP hot spots) were mapped ($n = 10$). Note that the most rostral and most caudal dye spots were separated by ~100 μm along this axis. ***D***, Transverse section of neonatal rat medulla illustrating the location of the pontamine sky blue dye spot (arrow), relative to scNA and NK1R immunolabeling. ***E***, ***F***, High magnification images of the boxed regions in ***D***. Abbreviations: NTS, nucleus of the solitary tract; ROb, raphe obscurus; SpV, spinal trigeminal nucleus. Scale bar, 100 μm (in all panels).

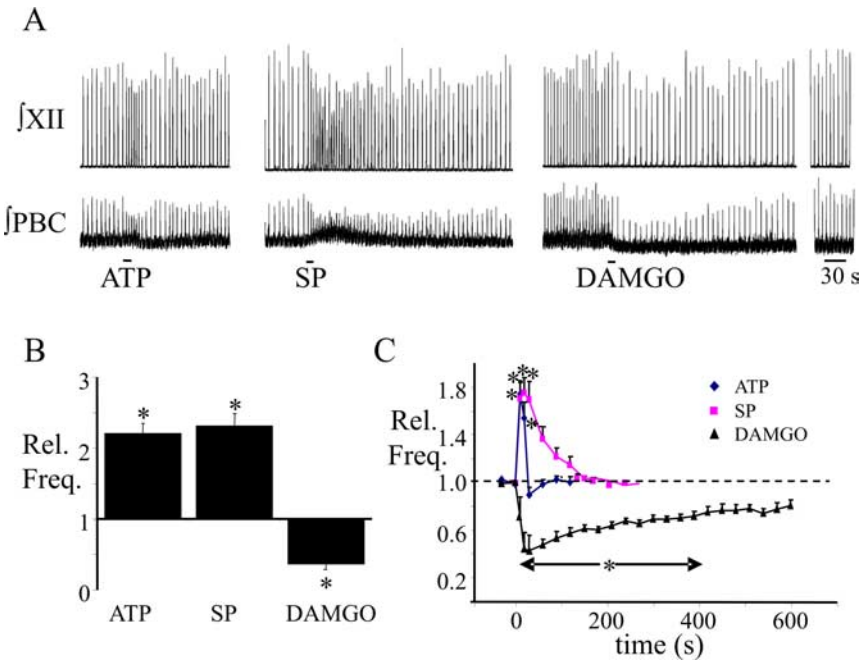

Figure 5. The ATP hotspot is sensitive to NK1 and μ-opioid receptor activation. ***A***, ∫XII nerve and ∫preBötC recordings illustrating the response to local application of ATP (0.1 mM), SP (1 μM), or DAMGO (50 μM) to the ATP hotspot. Group data ($n = 6$) illustrating the maximum frequency increase (***B***) and time course of responses (***C***) evoked by each agonist. *Significantly different from control. Error bars indicate SEM. Rel. Freq., Relative frequency.

transmission (Greer et al., 1991; Funk et al., 1993), was not affected by 500 μM PPADS. The antagonist TNP-ATP (bath applied, 0.01–10 μM), which is selective for $P2X_1$, $P2X_3$, and $P2X_{2/3}$Rs in the nanomolar range, but can also affect PX_2, $P2X_4$, $P2X_6$, $P2X_{1/5}$, and $P2X_7$Rs at concentrations several orders of magnitude higher (Lambrecht, 2000; Jones et al., 2004), was without effect on the increase of frequency produced by 0.1 mM ATP (Fig. 8*F*) ($n = 4$).

The agonist potency profile, in which ATP ≈ 2MeSATP (Fig. 8) ≈ ATPγs (Fig. 11) ⋙ UTP (Fig. 8) ≈ $\alpha\beta$meATP (Fig. 8) (Kawamura et al., 2004), and lack of efficacy of the antagonists suramin and PPADS at low concentrations were most consistent with a $P2Y_1$-mediated effect. $P2Y_1$R involvement was then tested by applying the $P2Y_1$R agonist 2MeSADP (0.1 mM) into the preBötC. It caused a 2.6 ± 0.2-fold increase in frequency that was similar in magnitude (2.3 ± 0.1-fold), but of greater duration, compared with the ATP effect (Fig. 9*A*,*B*) ($n = 12$). Frequency remained significantly elevated for at least 30 s after 2MeSADP application, but only for 20 s after ATP application (Fig. 9*B*). Moreover, local microinjection of the $P2Y_1$ selective antagonist MRS2179 (Camaioni et al., 1998) to the preBötC for 2 min before agonist microinjection significantly attenuated the effects of ATP and 2MeSADP on burst frequency (Fig. 9*C–F*). At 50 μM MRS2179, the ATP potentiation fell from a 2.44 ± 0.2-fold increase to 1.45 ± 0.2 (i.e., MRS2179 decreased the response to 0.27 ± 0.10 of the control ATP increase) (Fig. 9*D*) ($n = 9$). Increasing the concentration of MRS2179 to 100 μM in a separate series of experiments did not cause a greater reduction in the frequency response (the frequency increase was only 0.23 ± 0.07 of the control ATP increase) (Fig. 9*D*) ($n = 8$). In contrast, the MRS2179 inhibition of the 2MeSADP-mediated frequency increase ($n = 8$) was dose dependent. Frequency increases were 0.71 ± 0.09 and 0.45 ± 0.13 of the control 2MeSADP increase in the presence of 50 and 100 μM MRS2179, respectively (Fig. 9*F*) ($n = 6$).

The potential for $P2Y_1$R involvement in the ATP-evoked frequency increase was also examined using double-labeling fluorescent immunohistochemistry to characterize the pattern of $P2Y_1$R expression relative to NK1R immunolabeling. The preBötC was identified as a cluster of neurons located ventrolateral to scNA that had reasonably strong immunolabeling for the NK1R (Fig. 10*A*,*C*). $P2Y_1$R labeling was found in the preBötC region and colocalized with NK1R immunolabeling in some preBötC neurons (Fig. 10*B*,*D*) ($n = 3$).

The post-ATP frequency inhibition requires ATP hydrolysis

As described previously, the frequency response to ATP in the preBötC is biphasic. An initial increase is followed in most cases

by a short-lasting decrease in frequency (Fig. 1*A*). Given that extracellular ATP is rapidly hydrolyzed by ectonucleotidases to ADP and adenosine (Zimmermann, 2000, 2001), which is an inhibitory modulator of respiratory frequency (Herlenius et al., 1997; Herlenius and Lagercrantz, 1999), we tested whether the post-ATP inhibition of frequency results from the hydrolysis of ATP. We compared the effects on frequency of microinjecting into the preBötC ATP and ATPγs, a nonhydrolysable analog of ATP. When applied at the same site, ATP (0.1 mM) and ATPγs (0.1 mM) evoked similar, rapid increases in respiratory frequency that peaked at 3.30 ± 0.3-fold or 3.10 ± 0.3-fold greater than control, respectively (Fig. 11*A*,*B*) ($n = 7$). ATP responses, however, were shorter in duration (Fig. 11*C*). Frequency remained significantly greater than control for only 15 s after the onset of ATP application compared with 40 s after ATPγs (Fig. 11*C*). In addition, the post-ATP decrease in burst frequency (0.79 ± 0.06-fold) that followed ATP application was not observed after ATPγs.

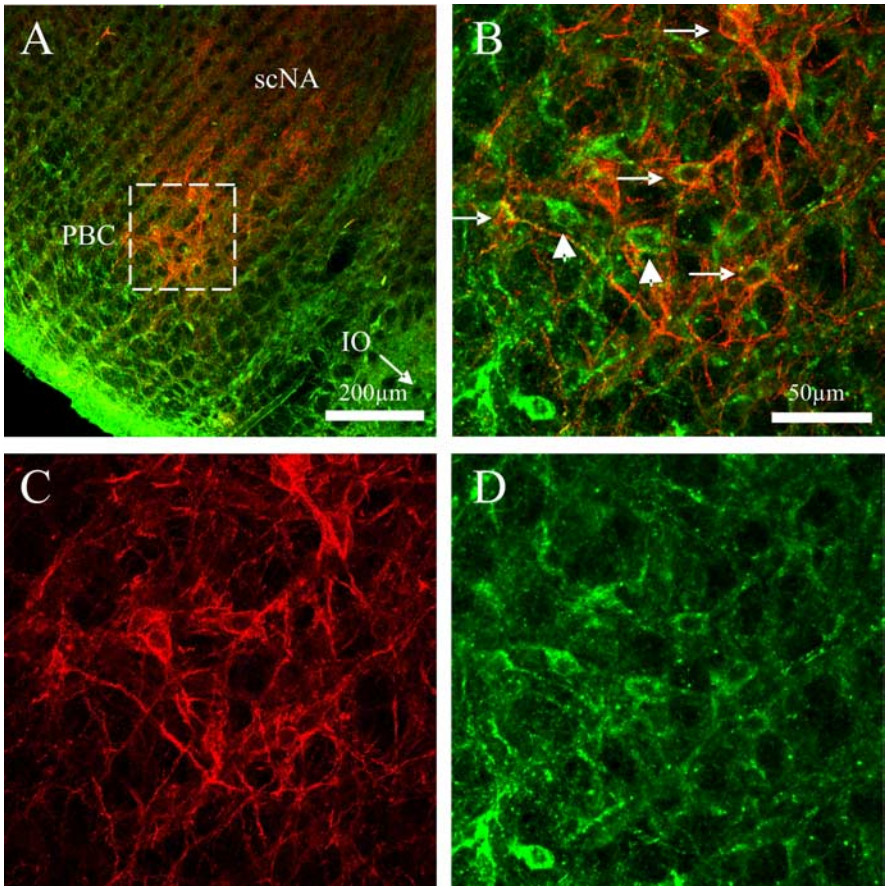

Figure 6. $P2X_2$ and NK1 receptor immunolabeling are present in the preBötC (PBC). ***A***, Low-power (10×) image of a medullary slice illustrating immunolabeling for NK1R (red) and $P2X_2R$ (green) in the scNA and PBC. ***B–D***, Higher-power (40×) images of NK1R (***C***; red) and $P2X_1$ (***D***; green) immunolabeling in the preBötC region (boxed area in ***A***) alone (***C***, ***D***) and overlaid (***B***). The arrowheads in ***B*** indicate $P2X_2R$-expressing preBötC neurons. The arrows indicate $P2X_2$ and NK1R colocalization, seen as yellow, in some preBötC neurons.

Involvement of endogenously released ATP

To determine whether endogenous ATP modulates respiratory rhythm in the medullary slice preparation, we examined the effects on baseline inspiratory burst frequency of several P2R antagonists or allosteric modulators. Most drugs were without effect on frequency (data not shown), including the following: (1) PPADS (bath-applied at 50 μM; $n = 5$), (2) TNP-ATP ($P2X_1$ and $P2X_3$ antagonist; bath-applied at 0.01–10 μM; $n = 4$), and (3) MRS2179 ($P2Y_1$ antagonist; locally microinjected at 100 μM into the preBötC for 2 min, $n = 14$; or bath-applied at 50 μM, $n = 4$).

In contrast, suramin (50 μM) significantly reduced inspiratory frequency by a factor of 0.33 ± 0.06 (from 17.1 ± 0.9 to 11.5 ± 0.6 cycles/min; $n = 4$) (Figure 12) when applied to the bath. The suramin effect did not wash out, but this was unlikely to reflect nonspecific rundown in activity, because inspiratory frequency did not change significantly over the same period in time-matched controls ($n = 6$) (Fig. 12). Cu^{2+}, an allosteric modulator of $P2X_2Rs$ (Xiong et al., 1999), also evoked a significant increase in frequency at all three concentrations. Frequency increased 1.63 ± 0.12-fold [from 13.8 ± 0.8 to a maximum of 22.5 ± 2.1 cycles/min at 25 μM Cu^{2+} ($CuCl_2$)] and recovered to control levels after washout ($n = 7$) (Fig. 12).

Discussion

Activation of P2Rs in the preBötC increases inspiratory frequency

The preBötC is a region in the VLM that is essential and sufficient for inspiratory rhythm generation (Smith et al., 1991; Feldman and Del Negro, 2006). Three lines of evidence from this study support that ATP acts with maximum potency in the preBötC to increase frequency. First, the pontamine sky blue-labeled ATP hotspot maps to a region anatomically consistent with the preBötC (Smith et al., 1991; Funk et al., 1993; Pagliardini et al., 2003; Feldman and Del Negro, 2006). Second, dye spots colocalize with regions of moderate NK1R immunolabeling, and NK1-immunoreactive preBötC neurons double label for $P2X_2$ and $P2Y_1$ receptors. preBötC markers include NK1, μ-opioid, and somatostatin receptor labeling (Gray et al., 1999; Stornetta et al., 2003), but NK1R labeling is used most extensively (Gray et al., 1999, 2001; Guyenet and Wang, 2001; Wang et al., 2001; Guyenet et al., 2002; Pagliardini et al., 2003, 2005). It is not exclusive to preBötC neurons but remains useful, because preBötC staining is greater than in surrounding regions. In addition, NK1R-expressing preBötC neurons are essential for rhythm generation (Gray et al., 2001; Pagliardini et al., 2003; Wenninger et al., 2004; McKay et al., 2005). Third, activation of NK1 or μ-opioid receptors in the ATP hotspot potently increases or decreases, respectively, respiratory frequency. These responses functionally identify the preBötC (Johnson et al., 1996; Gray et al., 1999) and, combined with histological and immunochemical data, provide compelling evidence that the ATP hotspot corresponds to the preBötC.

The effects of ATP in the preBötC on rhythm were remarkably consistent in neonates *in vitro*. They were not, however, consistent with *in vivo* studies that indicate that ATP [at high concentrations (20 mM)] (Thomas and Spyer, 2000; Gourine et al., 2003) excites inspiratory neurons, but blocks phrenic nerve output causing apnea (Spyer and Thomas, 2000; Thomas et al., 2001;

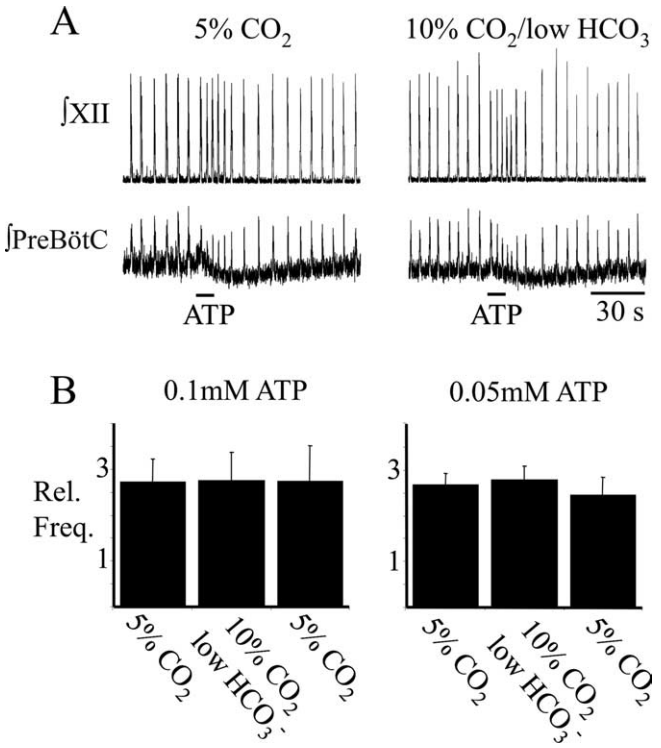

Figure 7. ATP potentiation of frequency is not affected by the pH of the aCSF. ***A***, ∫XII and ∫preBötC recordings illustrating the effects on inspiratory-related output in a single slice of locally applying ATP (0.05 mM) to the preBötC at pH 7.45 ± 0.01 (5% CO_2) and pH 7.04 ± 0.02 (10% CO_2/low HCO_3^-). ***B***, Histogram of group data illustrating the maximum frequency response evoked by locally applying ATP (0.1 and 0.05 mM) under conditions of high (5% CO_2) and low (10% CO_2/low HCO_3^-) extracellular pH. Error bars indicate SEM. Rel. Freq., Relative frequency.

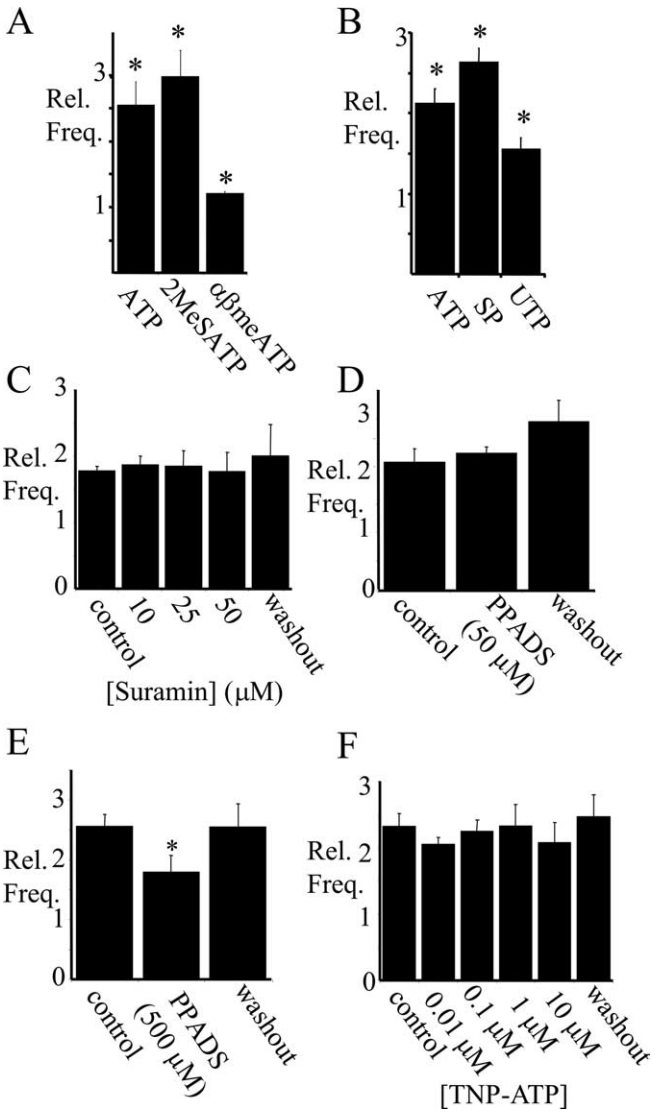

Figure 8. Effect of P2 receptor agonists and antagonists. ***A***, Histogram of group data illustrating the response to local application within the hotspot of ATP (0.1 mM; $n = 9$), 2MeSATP (0.1 mM; $n = 4$), and $\alpha\beta$meATP (0.1 mM; $n = 5$). ***B***, Histogram of group data illustrating the effects on frequency of locally applying ATP (0.1 mM), UTP (0.1 mM), and SP (1 μM) into the preBötC of the same medullary slice ($n = 6$). Group data illustrating that bath application of suramin (10–50 μM; $n = 4$) (***C***), PPADS (50 μM; $n = 5$) (***D***), or TNP-ATP (0.01–10 μM; $n = 5$) (***F***) had no significant effect on the frequency response evoked by locally applying ATP (0.1 mM) to the preBötC. Group data illustrating local application of PPADS (500 μM; 120 s total duration; $n = 5$) (***E***) starting 90 s before the ATP injection reversibly inhibited the ATP-evoked increase in frequency. *Significantly different from control. Error bars indicate SEM. Rel. Freq., Relative frequency.

Gourine et al., 2005b). Factors underlying these differences are not known. *In vivo* effects may represent depolarization block because 10 mM ATP also arrests rhythm *in vitro* (Lorier et al., 2004). However, it may also reflect development of purinergic signaling (Collo et al., 1996; Kanjhan et al., 1999; Brosenitsch et al., 2005) in neurons and glia that contribute to ATP responses (Fields and Burnstock, 2006) but are immature at birth (Liu et al., 2002). Sites of ATP application *in vivo* and *in vitro* may also have differed.

P2R subtypes underlying the ATP-mediated frequency increase

Despite P2XR immunolabeling of VLM neurons, $P2X_2R$ labeling of inspiratory neurons and NK1R-labeled preBötC neurons, and suramin-sensitive, ATP-evoked increases in inspiratory neuron discharge (Kanjhan et al., 1999; Yao et al., 2000; Thomas et al., 2001; Gourine et al., 2003), the agonist/antagonist profiles do not support a major role for P2XRs in the ATP-evoked frequency increase. The $P2X_{1,3}R$ agonist $\alpha\beta$meATP had minor effects on frequency, whereas the $P2X_{1,3}R$ antagonist, TNP-ATP, did not block the ATP response. $P2X_2R$ subunits are also unlikely to play a dominant role, because $P2X_2$ subunit-containing P2XRs are potentiated by acidic shifts in pH, but acidification of the bathing solution did not affect the ATP response. It is important to emphasize caution when interpreting such negative data. Indeed, we cannot exclude the possibility that the pH sensitivity of $P2X_2$ receptors was somehow altered *in vitro*. However, we are confident that the pH changes generated in the tissue at the site of ATP injection were of sufficient magnitude and in the correct range to enhance currents of $P2X_2$ subunit-containing receptors. First, $P2X_2$ receptor currents almost double between pH levels of 7.1 and 6.8 (King et al., 1996). Second, tissue pH in medullary slices and en bloc preparations (Okada et al., 1993; Trapp et al., 1996; Voipio and Ballanyi, 1997) at a depth in the tissue of 150 μm, where ATP injections were made, is ~0.3 pH units lower than the aCSF. Thus, tissue pH likely decreased from ~7.15 to ~6.75. Insensitivity of the frequency response to low concentrations of suramin and PPADS further suggests that $P2X_2$ and $P2X_5$ receptors are not involved (Norenberg and Illes, 2000). A contribution of $P2X_4$ and $P2X_6$ receptors, which are less sensitive to suramin and PPADS (Norenberg and Illes, 2000), or heteromeric P2XRs

with unique pharmacology, remains possible. However, we established that $P2Y_1Rs$ are primarily responsible for the ATP-evoked frequency increase. The agonist (2MeSADP ≈ ATP ≈ 2MeSATP ≈ ATPγs ⋙ UTP ≈ αβmeATP) (Kawamura et al., 2004) and antagonist profiles were most consistent with $P2Y_1Rs$. The ATP frequency increase was highly sensitive only to the $P2Y_1R$ antagonist MRS2179 (Camaioni et al., 1998; von Kugelgen, 2005). Finally, preBötC neurons show $P2Y_1R$ IR or double-labeling for $P2Y_1$ and NK1R.

The cellular or synaptic mechanisms underlying the $P2Y_1R$-evoked frequency increase are not known. It could reflect activation of $P2Y_1$ receptors located on glia, postsynaptically on preBötC neurons, or presynaptically on terminals of glutamatergic, GABAergic, or modulatory neurons (Fields and Burnstock, 2006; Hussl and Boehm, 2006) that project to the preBötC.

Evidence of P2YR involvement in respiratory or motor control is limited. In rat, chemosensitive retrotrapezoid nucleus (RTN) cells are excited by P2YR activation (Mulkey et al., 2006), whereas in *Xenopus* tadpole swimming episodes are potentiated by $P2Y_1R$-like inhibition of a K^+ conductance (Brown and Dale, 2002). Ours is the first demonstration in the mammalian CNS of $P2Y_1R$ modulation of respiratory motor networks.

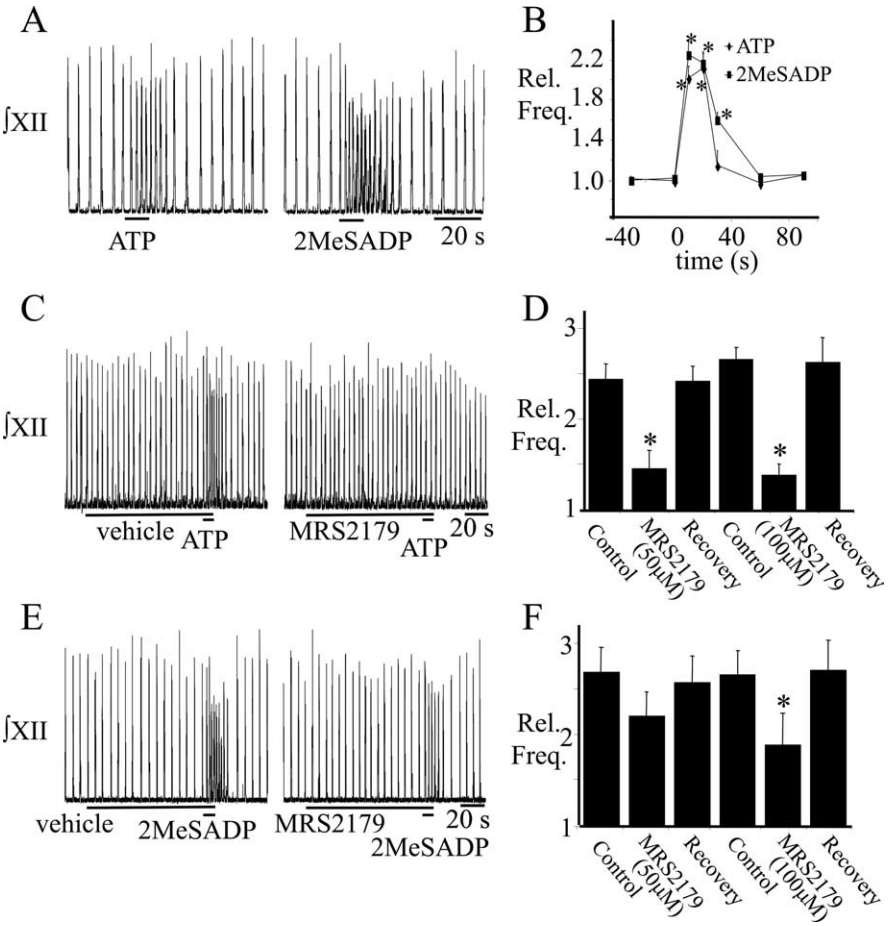

Figure 9. $P2Y_1$ receptor involvement in the ATP-induced frequency increase. ∫XII nerve recordings from a rhythmic medullary slice (***A***) and group data (***B***) ($n = 12$) comparing the responses evoked by applying ATP (0.1 mM) or the $P2Y_1$ receptor agonist, 2MeSADP (0.1 mM) to the preBötC. ***C***, ***E***, ∫XII nerve recordings illustrating that preapplication of MRS2179 (100 μM; 2 min) to the preBötC reduced the response to ATP (***C***) and 2MeSADP (***E***). Group data showing attenuation of the ATP (***D***) or 2MeSADP (***F***) response in the presence of 50 and 100 μM MRS2179 (ATP, $n = 9$ and 8 for 50 and 100 μM, respectively; 2MeSADP, $n = 8$ and 6 for 50 and 100 μM, respectively.) *Significantly different from control. Error bars indicate SEM. Rel. Freq., Relative frequency.

Implication of ATP hydrolysis

P2R signaling is complicated by a system of ectonucleotidases that hydrolyze extracellular ATP into adenosine (Dunwiddie et al., 1997; Zimmermann, 2000), which acts via P1Rs, in particular the A_1R, to inhibit transmitter release (Dunwiddie et al., 1997; Ralevic and Burnstock, 1998; Haas and Selbach, 2000). In respiratory networks, adenosine is clinically significant because it depresses ventilation (Herlenius et al., 1997; Herlenius and Lagercrantz, 1999; Mironov et al., 1999), and is implicated in the hypoxia-induced depression of ventilation (Yan et al., 1995) and apnea in newborns (Runold et al., 1989; Lopes et al., 1994). Our observation that the post-ATP decrease in frequency depends on ATP breakdown suggests that effects of ATP on rhythm will be determined by an interaction between P2 and P1 receptors. In other brain regions, P2–P1R interactions influence synaptic transmission (Kato et al., 2000; Kato and Shigetomi, 2001; Kawamura et al., 2004) and determine the dynamics of inspiratory motor responses to ATP (Funk et al., 1997a; Miles et al., 2002). Moreover, as seen here for respiratory activity, the time course of swimming episodes in tadpoles is determined by an interaction between a $P2Y_1R$-like excitatory mechanism and the degradation of ATP (Dale and Gilday, 1996; Brown and Dale, 2002). These data highlight the potential importance of ectonucleotidases and raise the possibility that regulation of these enzymes may provide an additional mechanism for controlling network activity.

Physiological role for P2R signaling in respiratory control

Although ATP acts as an excitatory neurotransmitter within many brain regions, including autonomic nuclei (Nieber et al., 1997; Scislo et al., 1998; Thomas et al., 1999; Gourine et al., 2003, 2005a), its physiological significance is only just emerging. In respiratory networks, ATP is important for peripheral (Rong et al., 2003) and central chemoreception (Gourine et al., 2005a,b). It is released in the brainstem during hypoxia or hypercapnia and stimulates respiratory activity (Gourine et al., 2005a,b). During hypercapnia, ATP is released from the ventrolateral surface of the medulla (Gourine et al., 2005b) where its stimulation of respiration may reflect an interaction between a P2YR-mediated increase and P2XR-mediated decrease in the excitability of pH-sensitive RTN neurons (Mulkey et al., 2006). During hypoxia, ATP is released from the ventrolateral surface of the medulla as well as the VRC. It stimulates respiratory frequency, reducing the secondary hypoxic depression of respiration (Gourine et al., 2005a). Our data indicate that this effect could be mediated, in whole or in part, by the activation of $P2Y_1Rs$ in the preBötC.

It is important to note that the lack of an effect of the $P2Y_1R$ antagonist, MRS2179, on baseline frequency does not exclude endogenous purinergic modulation of respiratory rhythm. Slices lack many potential sources of ATP including pontine noradrenergic cell groups (Nieber et al., 1997; Poelchen et al., 2001). It is

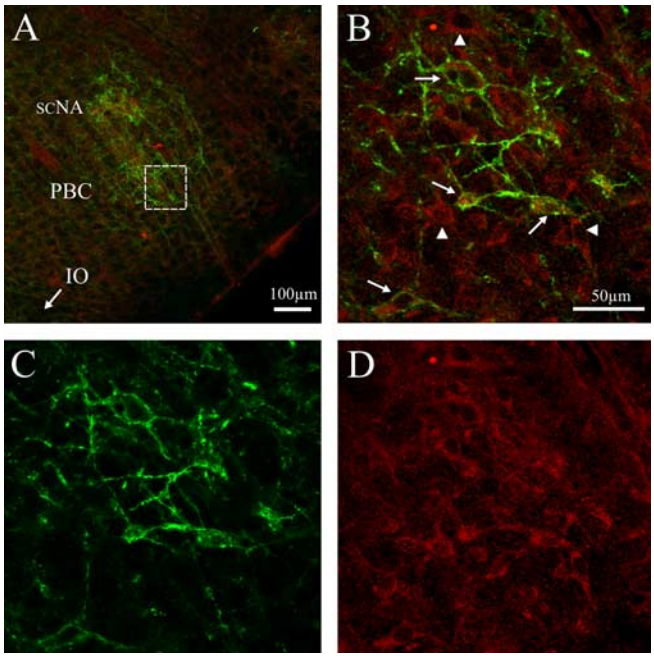

Figure 10. $P2Y_1$ and NK1 receptor immunolabeling are present in the preBötC (PBC). ***A***, Low-power (10×) image of a medullary slice illustrating immunolabeling for NK1R (green) and $P2Y_1R$ (red) in the scNA and preBötC. ***B–D***, Higher-power (40×) images of NK1R (***C***; green) and $P2Y_1R$ (***D***; red) immunolabeling in the preBötC region (boxed area in ***A***) alone (***C***, ***D***) and overlaid (***B***). The arrowheads in ***B*** indicate $P2Y_1R$-expressing preBötC neurons. The arrows indicate $P2Y_1$ and NK1R colocalization, seen as yellow, in some preBötC neurons.

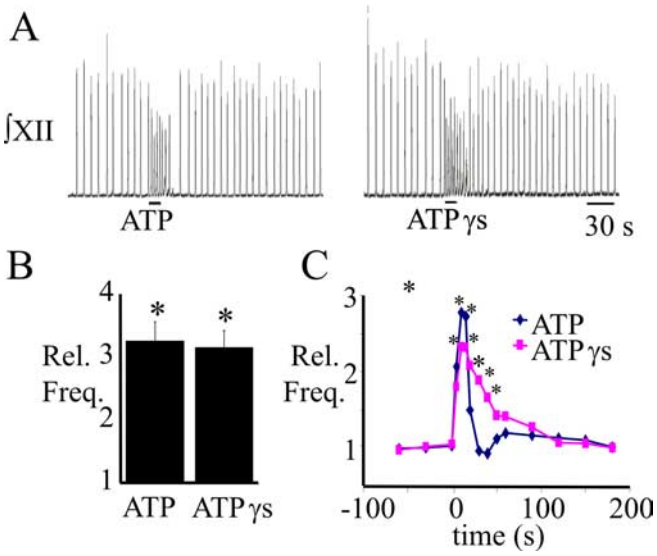

Figure 11. The post-ATP inhibition of inspiratory frequency requires ATP hydrolysis. ***A***, ∫XII nerve recordings illustrating the response to local application of ATP (0.1 mM) or ATPγs (0.1 mM) to the preBötC. Group data ($n = 7$) illustrating the maximum response (***B***) and time course (***C***) of the responses evoked by each agonist. *Significantly different from control. Error bars indicate SEM. Rel. Freq., Relative frequency.

also possible that ATP does not modulate baseline respiratory activity, but is released in response to specific stimuli such as hypercapnia or hypoxia (Gourine et al. 2005a, b) that cannot be reproduced *in vitro* [e.g., transmitters released during hypoxia *in vitro*, which represents a transition from hyperoxia to anoxia (Ramirez et al., 1997), may differ considerably from those released during hypoxia *in vivo*]. Another possibility is that endogenous purinergic modulation of rhythmic activity may not be limited to a direct, $P2Y_1R$-mediated preBötC effect, but an indirect action via P2XRs outside the preBötC. Some support for this is that Cu^{2+}, which potentiates $P2X_2R$ currents (Xiong et al., 1999), reversibly increased baseline frequency. Additionally, bath-applied suramin did not alter the frequency effects of ATP in the preBötC, but significantly reduced baseline rhythm. Although the nonspecific actions of these two agents demand cautious interpretation, these data and $P2Y_1R$ modulation of rhythm suggest that important future objectives will be to establish that the effects observed here in neonates persist into adulthood, and to identify the full compliment of stimuli that evoke ATP release from the different compartments of the respiratory network.

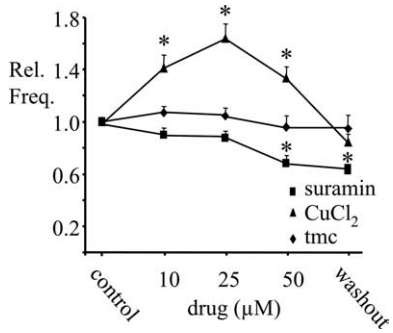

Figure 12. Effect of a P2R antagonist and allosteric modulator on baseline inspiratory frequency. Group data illustrating the effects on frequency of bath-applied suramin (10–50 μM; $n = 4$) or $CuCl_2$ (10–50 μM; $n = 6$) on baseline activity of rhythmically active medullary slices. Time-matched controls (tmc) ($n = 6$) show no change in frequency over the equivalent time period. *Significantly different from control. Error bars indicate SEM. Rel. Freq., Relative frequency.

In summary, recent data have established an endogenous role for ATP in central respiratory control; it is released during hypoxia from the brainstem and attenuates the secondary hypoxic depression of respiratory frequency (Gourine et al., 2005a). The significance of the present study is that it advances our understanding of mechanisms through which purinergic signaling can modulate respiratory rhythm by establishing that ATP potently increases respiratory frequency by activating $P2Y_1Rs$ in the preBötC.

References

Brosenitsch TA, Adachi T, Lipski J, Housley GD, Funk GD (2005) Developmental downregulation of $P2X_3$ receptors in motoneurons of the compact formation of the nucleus ambiguus. Eur J Neurosci 22:809–824.

Brown P, Dale N (2002) Modulation of K^+ currents in *Xenopus* spinal neurons by p2y receptors: a role for ATP and ADP in motor pattern generation. J Physiol (Lond) 540:843–850.

Camaioni E, Boyer JL, Mohanram A, Harden TK, Jacobson KA (1998) Deoxyadenosine bisphosphate derivatives as potent antagonists at P2Y1 receptors. J Med Chem 41:183–190.

Collo G, North RA, Kawashima E, Merlo-Pich E, Neidhart S, Surprenant A, Buell G (1996) Cloning of $P2X_5$ and $P2X_6$ receptors and the distribution and properties of an extended family of ATP-gated ion channels. J Neurosci 16:2495–2507.

Dale N, Gilday D (1996) Regulation of rhythmic movements by purinergic neurotransmitters in frog embryos. Nature 383:259–263.

Dunwiddie TV, Diao L, Proctor WR (1997) Adenine nucleotides undergo rapid, quantitative conversion to adenosine in the extracellular space in rat hippocampus. J Neurosci 17:7673–7682.

Feldman JL, Del Negro CA (2006) Looking for inspiration: new perspectives on respiratory rhythm. Nat Rev Neurosci 7:232–242.

Fields RD, Burnstock G (2006) Purinergic signalling in neuron-glia interactions. Nat Rev Neurosci 7:423–436.

Funk GD, Smith JC, Feldman JL (1993) Generation and transmission of

respiratory oscillations in medullary slices: role of excitatory amino acids. J Neurophysiol 70:1497–1515.

Funk GD, Kanjhan R, Walsh C, Lipski J, Comer AM, Parkis MA, Housley GD (1997a) P2 receptor excitation of rodent hypoglossal motoneuron activity *in vitro* and *in vivo*: a molecular physiological analysis. J Neurosci 17:6325–6337.

Funk GD, Parkis MA, Selvaratnam SR, Walsh C (1997b) Developmental modulation of glutamatergic inspiratory drive to hypoglossal motoneurons. Respir Physiol 110:125–137.

Gourine AV, Atkinson L, Deuchars J, Spyer KM (2003) Purinergic signalling in the medullary mechanisms of respiratory control in the rat: respiratory neurones express the $P2X_2$ receptor subunit. J Physiol (Lond) 552:197–211.

Gourine AV, Llaudet E, Dale N, Spyer KM (2005a) Release of ATP in the ventral medulla during hypoxia in rats: role in hypoxic ventilatory response. J Neurosci 25:1211–1218.

Gourine AV, Llaudet E, Dale N, Spyer KM (2005b) ATP is a mediator of chemosensory transduction in the central nervous system. Nature 436:108–111.

Gray PA, Rekling JC, Bocchiaro CM, Feldman JL (1999) Modulation of respiratory frequency by peptidergic input to rhythmogenic neurons in the preBotzinger complex. Science 286:1566–1568.

Gray PA, Janczewski WA, Mellen N, McCrimmon DR, Feldman JL (2001) Normal breathing requires preBotzinger complex neurokinin-1 receptor-expressing neurons. Nat Neurosci 4:927–930.

Greer JJ, Smith JC, Feldman JL (1991) Role of excitatory amino acids in the generation and transmission of respiratory drive in neonatal rat. J Physiol (Lond) 437:727–749.

Guyenet PG, Wang H (2001) Pre-Botzinger neurons with preinspiratory discharges "in vivo" express NK1 receptors in the rat. J Neurophysiol 86:438–446.

Guyenet PG, Sevigny CP, Weston MC, Stornetta RL (2002) Neurokinin-1 receptor-expressing cells of the ventral respiratory group are functionally heterogeneous and predominantly glutamatergic. J Neurosci 22:3806–3816.

Haas HL, Selbach O (2000) Functions of neuronal adenosine receptors. Naunyn Schmiedebergs Arch Pharmacol 362:375–381.

Herlenius E, Lagercrantz H (1999) Adenosinergic modulation of respiratory neurones in the neonatal rat brainstem in vitro. J Physiol (Lond) 518:159–172.

Herlenius E, Lagercrantz H, Yamamoto Y (1997) Adenosine modulates inspiratory neurons and the respiratory pattern in the brainstem of neonatal rats. Pediatr Res 42:46–53.

Horie M, Miyashita T, Watabe K, Takeda Y, Kawamura K, Kawano H (2000) Immunohistochemical localization of substance P receptors in the midline glia of the developing rat medulla oblongata with special reference to the formation of raphe nuclei. Brain Res Dev Brain Res 121:197–207.

Hussl S, Boehm S (2006) Functions of neuronal P2Y receptors. Pflügers Arch 452:538–551.

Illes P, Alexandre Ribeiro J (2004) Molecular physiology of P2 receptors in the central nervous system. Eur J Pharmacol 483:5–17.

Johnson SM, Smith JC, Feldman JL (1996) Modulation of respiratory rhythm in vitro: role of Gi/o protein-mediated mechanisms. J Appl Physiol 80:2120–2133.

Jones CA, Vial C, Sellers LA, Humphrey PP, Evans RJ, Chessell IP (2004) Functional regulation of P2X6 receptors by N-linked glycosylation: identification of a novel alpha beta-methylene ATP-sensitive phenotype. Mol Pharmacol 65:979–985.

Kanjhan R, Housley GD, Burton LD, Christie DL, Kippenberger A, Thorne PR, Luo L, Ryan AF (1999) Distribution of the $P2X_2$ receptor subunit of the ATP-gated ion channels in the rat central nervous system. J Comp Neurol 407:11–32.

Kato F, Shigetomi E (2001) Distinct modulation of evoked and spontaneous EPSCs by purinoceptors in the nucleus tractus solitarii of the rat. J Physiol (Lond) 530:469–486.

Kato T, Hayashi F, Tatsumi K, Kuriyama T, Fukuda Y (2000) Inhibitory mechanisms in hypoxic respiratory depression studied in an in vitro preparation. Neurosci Res 38:281–288.

Kawamura M, Gachet C, Inoue K, Kato F (2004) Direct excitation of inhibitory interneurons by extracellular ATP mediated by $P2Y_1$ receptors in the hippocampal slice. J Neurosci 24:10835–10845.

King BF, Ziganshina LE, Pintor J, Burnstock G (1996) Full sensitivity of $P2X_2$ purinoceptor to ATP revealed by changing extracellular pH. Br J Pharmacol 117:1371–1373.

King BF, Wildman SS, Ziganshina LE, Pintor J, Burnstock G (1997) Effects of extracellular pH on agonism and antagonism at a recombinant P2X2 receptor. Br J Pharmacol 121:1445–1453.

Lambrecht G (2000) Agonists and antagonists acting at P2X receptors: selectivity profiles and functional implications. Naunyn Schmiedebergs Arch Pharmacol 362:340–350.

Liu G, Feldman JL, Smith JC (1990) Excitatory amino acid-mediated transmission of inspiratory drive to phrenic motoneurons. J Neurophysiol 64:423–436.

Liu Y, Wu Y, Lee JC, Xue H, Pevny LH, Kaprielian Z, Rao MS (2002) Oligodendrocyte and astrocyte development in rodents: an in situ and immunohistological analysis during embryonic development. Glia 40:25–43.

Lopes JM, Davis GM, Mullahoo K, Aranda JV (1994) Role of adenosine in the hypoxic ventilatory response of the newborn piglet. Pediatr Pulmonol 17:50–55.

Lorier AR, Robinson DM, Giles R, Greenwood D, Lipski J, Housley GD, Funk GD (2002) Modulation of respiratory rhythm generating networks by ATP. Soc Neurosci Abstr 28:173.8.

Lorier AR, Peebles K, Brosenitsch T, Robinson DM, Housley GD, Funk GD (2004) P2 receptors modulate respiratory rhythm but do not contribute to central CO_2 sensitivity in vitro. Respir Physiol Neurobiol 142:27–42.

McKay LC, Janczewski WA, Feldman JL (2005) Sleep-disordered breathing after targeted ablation of preBotzinger complex neurons. Nat Neurosci 8:1142–1144.

Miles GB, Parkis MA, Lipski J, Funk GD (2002) Modulation of phrenic motoneuron excitability by ATP: consequences for respiratory-related output *in vitro.* J Appl Physiol 92:1899–1910.

Mironov SL, Langohr K, Richter DW (1999) A1 adenosine receptors modulate respiratory activity of the neonatal mouse via the cAMP-mediated signaling pathway. J Neurophysiol 81:247–255.

Mulkey DK, Mistry AM, Guyenet PG, Bayliss DA (2006) Purinergic P2 receptors modulate excitability but do not mediate pH sensitivity of RTN respiratory chemoreceptors. J Neurosci 26:7230–7233.

Nicholson C (1985) Diffusion from an injected volume of a substance in brain tissue with arbitrary volume fraction and tortuosity. Brain Res 333:325–329.

Nieber K, Poelchen W, Illes P (1997) Role of ATP in fast excitatory synaptic potentials in locus coeruleus neurones of the rat. Br J Pharmacol 122:423–430.

Norenberg W, Illes P (2000) Neuronal P2X receptors: localisation and functional properties. Naunyn Schmiedebergs Arch Pharmacol 362:324–339.

North RA (2002) Molecular physiology of P2X receptors. Physiol Rev 82:1013–1067.

North RA, Surprenant A (2000) Pharmacology of cloned P2X receptors. Annu Rev Pharmacol Toxicol 40:563–580.

North RA, Verkhratsky A (2006) Purinergic transmission in the central nervous system. Pflügers Arch 452:479–485.

Okada Y, Muckenhoff K, Holtermann G, Acker H, Scheid P (1993) Depth profiles of pH and PO_2 in the isolated brain stem-spinal cord of the neonatal rat. Respir Physiol 93:315–326.

Pagliardini S, Ren J, Greer JJ (2003) Ontogeny of the pre-Botzinger complex in perinatal rats. J Neurosci 23:9575–9584.

Pagliardini S, Adachi T, Ren J, Funk GD, Greer JJ (2005) Fluorescent tagging of rhythmically active respiratory neurons within the pre-Botzinger complex of rat medullary slice preparations. J Neurosci 25:2591–2596.

Poelchen W, Sieler D, Wirkner K, Illes P (2001) Co-transmitter function of ATP in central catecholaminergic neurons of the rat. Neuroscience 102:593–602.

Prasad M, Fearon IM, Zhang M, Laing M, Vollmer C, Nurse CA (2001) Expression of P2X2 and P2X3 receptor subunits in rat carotid body afferent neurones: role in chemosensory signalling. J Physiol (Lond) 537:667–677.

Ralevic V, Burnstock G (1998) Receptors for purines and pyrimidines. Pharmacol Rev 50:413–492.

Ramirez JM, Quellmalz UJ, Wilken B (1997) Developmental changes in the hypoxic response of the hypoglossus respiratory motor output in vitro. J Neurophysiol 78:383–392.

Rong W, Gourine AV, Cockayne DA, Xiang Z, Ford AP, Spyer KM, Burnstock G (2003) Pivotal role of nucleotide $P2X_2$ receptor subunit of the ATP-

gated ion channel mediating ventilatory responses to hypoxia. J Neurosci 23:11315–11321.

Runold M, Lagercrantz H, Prabhakar NR, Fredholm BB (1989) Role of adenosine in hypoxic ventilatory depression. J Appl Physiol 67:541–546.

Scislo TJ, Ergene E, O'Leary DS (1998) Impaired arterial baroreflex regulation of heart rate after blockade of P2-purinoceptors in the nucleus tractus solitarius. Brain Res Bull 47:63–67.

Smith JC, Ellenberger HH, Ballanyi K, Richter DW, Feldman JL (1991) Pre-Botzinger complex: a brainstem region that may generate respiratory rhythm in mammals. Science 254:726–729.

Spyer KM, Thomas T (2000) Sensing arterial CO_2 levels: a role for medullary P2X receptors. J Auton Nerv Syst 81:228–235.

Stornetta RL, Rosin DL, Wang H, Sevigny CP, Weston MC, Guyenet PG (2003) A group of glutamatergic interneurons expressing high levels of both neurokinin-1 receptors and somatostatin identifies the region of the pre-Botzinger complex. J Comp Neurol 455:499–512.

Telgkamp P, Ramirez JM (1999) Differential responses of respiratory nuclei to anoxia in rhythmic brain stem slices of mice. J Neurophysiol 82:2163–2170.

Thomas T, Spyer KM (2000) ATP as a mediator of mammalian central CO_2 chemoreception. J Physiol (Lond) 523:441–447.

Thomas T, Ralevic V, Gadd CA, Spyer KM (1999) Central CO_2 chemoreception: a mechanism involving P2 purinoceptors localized in the ventrolateral medulla of the anaesthetized rat. J Physiol (Lond) 517:899–905.

Thomas T, Ralevic V, Bardini M, Burnstock G, Spyer KM (2001) Evidence for the involvement of purinergic signalling in the control of respiration. Neuroscience 107:481–490.

Trapp S, Luckermann M, Brooks PA, Ballanyi K (1996) Acidosis of rat dorsal vagal neurons in situ during spontaneous and evoked activity. J Physiol (Lond) 496:695–710.

Voipio J, Ballanyi K (1997) Interstitial PCO_2 and pH, and their role as chemostimulants in the isolated respiratory network of neonatal rats. J Physiol (Lond) 499:527–542.

von Kugelgen I (2005) Pharmacological profiles of cloned mammalian P2Y-receptor subtypes. Pharmacol Ther 110:415–432.

von Kugelgen I, Wetter A (2000) Molecular pharmacology of P2Y-receptors. Naunyn Schmiedebergs Arch Pharmacol 362:310–323.

Wang H, Stornetta RL, Rosin DL, Guyenet PG (2001) Neurokinin-1 receptor-immunoreactive neurons of the ventral respiratory group in the rat. J Comp Neurol 434:128–146.

Wenninger JM, Pan LG, Klum L, Leekley T, Bastastic J, Hodges MR, Feroah T, Davis S, Forster HV (2004) Small reduction of neurokinin-1 receptor-expressing neurons in the pre-Botzinger complex area induces abnormal breathing periods in awake goats. J Appl Physiol 97:1620–1628.

Xiong K, Peoples RW, Montgomery JP, Chiang Y, Stewart RR, Weight FF, Li C (1999) Differential modulation by copper and zinc of P2X2 and P2X4 receptor function. J Neurophysiol 81:2088–2094.

Yan S, Laferriere A, Zhang C, Moss IR (1995) Microdialyzed adenosine in nucleus tractus solitarii and ventilatory response to hypoxia in piglets. J Appl Physiol 79:405–410.

Yao ST, Barden JA, Finkelstein DI, Bennett MR, Lawrence AJ (2000) Comparative study on the distribution patterns of $P2X_1$-$P2X_6$ receptor immunoreactivity in the brainstem of the rat and the common marmoset (*Callithrix jacchus*): association with catecholamine cell groups. J Comp Neurol 427:485–507.

Zimmermann H (2000) Extracellular metabolism of ATP and other nucleotides. Naunyn Schmiedebergs Arch Pharmacol 362:299–309.

Zimmermann H (2001) Ectonucleotidases: some recent developments and a note on nomenclature. Drug Dev Res 52:44–56.